



## Fe<sub>16</sub>Al<sub>14</sub>B<sub>2</sub> phase in Fe–Al alloys

M. F. CHISHOLM†, G. DUSCHER

Solid State Division, Oak Ridge National Laboratory, Oak Ridge,  
Tennessee 37831, USA

LIXIN PANG and K. S. KUMAR

Division of Engineering, Brown University, Providence, Rhode Island 02912,  
USA

[Received 13 October 1999 and accepted in revised form 7 February 2000]

### ABSTRACT

The atomic structure and composition of a recently reported second phase found in Fe–Al alloys with small B and C additions have been determined using a combination of *Z*-contrast imaging and electron-energy-loss spectroscopy. The structure of this ordered tetragonal precipitate is found to be closely related to the B2 structure of the matrix. The derived structure and electron-energy-loss spectroscopy indicate that the phase is a new low-metalloid-content boride with B occupying specific interstitial sites.

### §1. INTRODUCTION

Fe–Al alloys with 40–50 at.% Al have an impressive combination of oxidation and sulphidation resistance, low density and low cost and are thus considered as possible substitutes for stainless steels. However, before these materials can be used in structural applications, the fracture characteristics of the alloy's grain boundaries need to be improved. Small additions of C and B have been considered and the resulting properties have been reported (Crimp and Vedula 1986, Liu and George 1990, Pang and Kumar 1997b). B is found to prevent intergranular fracture in Fe-rich alloys and to mitigate environmental embrittlement, although the improvement is not as dramatic as is seen with Ni<sub>3</sub>Al alloyed with B. B segregates to the grain boundaries in Fe–Al alloys and boride precipitates at the boundaries and within the grains have been observed. Gaydosh *et al.* (1989) concluded that the borides were Fe<sub>2</sub>B with a bct ( $a = 5.15 \text{ \AA}$  and  $c = 4.25 \text{ \AA}$ ). More recently, another phase has been detected in these B-containing alloys, and from electron diffraction patterns it has been determined that the phase is tetragonal with lattice parameters  $a = 11.56 \text{ \AA}$  and  $c = 2.89 \text{ \AA}$  (Pang and Kumar 1997a Pierron and Baker 1997). The phase was found to have an orientation relationship with B2 matrix in which

$$(001)_{\text{B2}} // (001)_{\text{boride}}; [001]_{\text{B2}} // [001]_{\text{boride}}.$$

This phase is only seen in Fe–Al alloys containing B. Therefore it is reasonable to assume that the phase contains B and that this phase may contribute to the increased

† Email: chisholmmf@ornl.gov.

strength observed with B additions (Baker and Gaydos 1986, Baker *et al.* 1998). The effect of heat treatment on the formation and stability of this phase (designated  $\nu$ ) has recently been reported (Pang and Kumar 1998).

In this paper, we report the composition and atomic arrangement in the  $\nu$  phase as determined using a combination of *Z*-contrast imaging and electron-energy-loss spectroscopy (EELS).

## §2. EXPERIMENTAL PROCEDURE

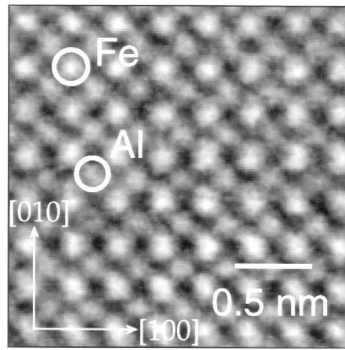
The Fe–Al–B–C ingot was obtained by vacuum induction melting and hot extruded with a 16:1 area-reduction ratio at 1000°C. Chemical analysis of the extruded rod yielded Fe–40 at.% Al–0.53 at.% B–0.7 at.% C. The as-extruded material was heat treated at 1150°C for 30 min and then air cooled to room temperature. Foils for electron microscopy were prepared by jet polishing in a 20% HNO<sub>3</sub> in methanol solution at –26°C and 15 V. Subsequent short-time ion milling with 1 kV Ar was used to expose new thin areas.

The high-resolution *Z*-contrast technique was used to form composition-sensitive images in a scanning transmission electron microscope (VG Microscopes HB603U) operated at 300 kV. *Z*-contrast images were formed by scanning a 0.126 nm electron beam (full width at half-maximum) across the specimen and recording the transmitted electrons scattered to large angles with an annular detector (inner detector angle, about 45 mrad). The *Z*-contrast image gives a directly interpretable map of the columnar scattering cross-section in which the resolution is limited by the size of the electron probe (Jesson and Pennycook 1993, Nellist and Pennycook 1999). High-spatial-resolution EELS was used to identify and quantify the elements in the precipitates. Spectra were collected using a VG Microscopes HB501UX scanning transmission electron microscope fitted with a high-sensitivity parallel EELS system.

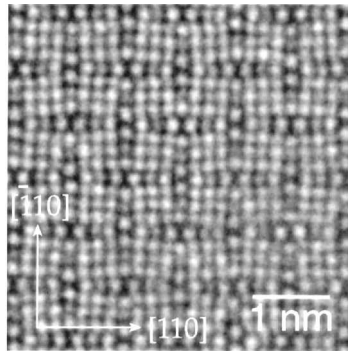
## §3. RESULTS

Conventional transmission electron microscopy revealed the presence of four different second phases in the as-extruded B2 FeAl matrix. Previous work (Pang and Kumar 1997a) has identified the three largest types of particle to be Fe<sub>2</sub>B, graphite and Fe<sub>2</sub>AlC<sub>0.5</sub>. In addition to these, a relatively small rod-like precipitate with an approximately square cross-section is seen. The long axis of the rods lie along orthogonal  $\langle 100 \rangle$  directions of the FeAl matrix. These precipitates are normally associated with a matrix stacking fault on  $\{001\}$  planes. This fault extends through the precipitate along the diagonal of the square cross-section of the rod. The sides of the approximately square precipitate cross-section are aligned along the  $\{110\}$  matrix planes. Selected-area diffraction confirms that the precipitates examined in this investigation have the same structure as those detected earlier. The phase is tetragonal with  $a_\nu = 4a_{\text{FeAl}}$  and  $c_\nu = a_{\text{FeAl}}$  ( $a_{\text{FeAl}} = 0.289$  nm) and is oriented with respect to the matrix such that  $[100]_\nu // [100]_{\text{FeAl}}$  and  $(001)_\nu // (001)_{\text{FeAl}}$ .

Figure 1(a) shows an atomic resolution *Z*-contrast image of the  $\langle 100 \rangle$  projection of the FeAl matrix, an ordered bcc-type structure in which one atom type sits at the corners of the cubic unit cell and the other occupies the body centre. The bright features correspond to the positions of the atomic columns; the brighter features correspond to the Fe columns and the less intense features correspond to the Al columns. Figure 1(b) is a *Z*-contrast image of the  $[001]$  projection of a  $\nu$ -phase precipitate, looking down the long dimension of the rod-like precipitates. One of



(a)



(b)

Figure 1. (a) Z-contrast image of the  $\langle 100 \rangle$  projection of the FeAl matrix. The bright features correspond to positions of atomic columns; the brightest features correspond to the Fe columns and the less intense features correspond to the Al columns. (b) Z-contrast image of the  $[001]$  projection of a  $\nu$ -phase precipitate. The severe distortions of the  $\{110\}$  planes of the precipitate are most obvious when the image is sighted along vertical or horizontal rows of atoms.

the most obvious features of the image is the seemingly complicated chequered pattern produced by large planar distortions in the precipitate. However, the structure responsible for this pattern is closely related to the B2 structure of the FeAl matrix. This is easier to discern by looking at the interface between the precipitate and the bulk B2 phase (figure 2(a)). No misfit dislocations were detected at the precipitate–matrix interface and, thus, the precipitates are coherent with the B2 matrix. In the FeAl matrix, individual  $\{001\}$  planes are composed of a single element and alternate Fe and Al. It can be seen that Fe planes continue across the matrix–precipitate interface (allowing for the distortions seen in the precipitate). The matrix Al planes also persist in the precipitate with one modification; in the precipitate, every fourth Al column is missing. The images suggest that the precipitate phase is derived fairly simply from the host B2 phase. The precipitate unit cell can be thought of as a modified  $4 \times 4 \times 1$  block of B2 cells (see the schematic diagram in figure 2(b)). (Note that, although the periodicity along the projection direction is not obvious from this single view, the images of the orthogonal  $\langle 100 \rangle$  projection and their corresponding electron diffraction patterns indicate that the periodicity in the

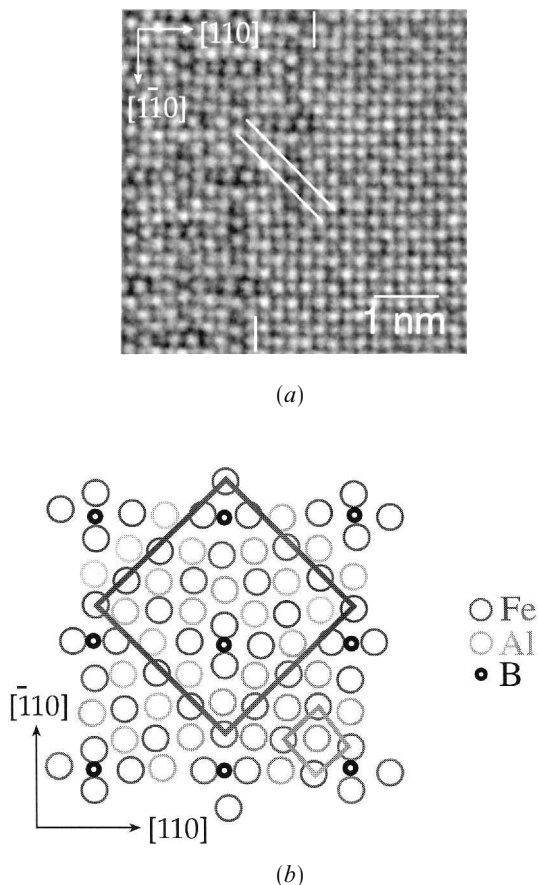


Figure 2. (a) Z-contrast image of the coherent interface between the precipitate and the bulk B2 phase (the interface is between the white vertical lines at the top and bottom of the image). It can be seen that Fe planes (e.g. under the diagonal white lines) continue across the matrix-precipitate interface. The matrix Al planes also persist in the precipitate with one modification; in the precipitate, every fourth Al column is missing. (b) Schematic diagram of the  $[001]$  projection of the  $\nu$  phase. The large dark square outlines the unit cell of the  $\nu$  phase. The smaller lighter square outlines the FeAl unit cell. B, which is not detected in the images, is assumed to be in one of the two sixfold trigonal prism sites of the diamond-like units. This uncertainty in the exact position is reflected by placing the B in the centre of the diamond (between the two likely sites).

$\langle 100 \rangle$  direction is the same as that of the B2 matrix.) The modification involves removing the Al column from two of the 16 B2 units, one from the middle unit of this  $4 \times 4$  block and the other from one corner. In these cells with missing Al, the two Fe columns at opposite corners of the cell move together along one cell diagonal, forming a diamond-like configuration. Thus, the  $\nu$ -phase unit cell is composed of 14 B2 cells and two diamond units. These diamond units produce rather severe distortions in the surrounding B2 units seen most easily by looking at the image at a glancing angle along  $\langle 110 \rangle$  directions. The precipitate distributes the distortions in orthogonal directions by alternating the orientation of the two diamond units in each precipitate unit cell.

The diamond-like features, obvious in the [001] projection of the precipitate, are reminiscent of structural units found in Fe<001> tilt grain boundaries (Vitek *et al.* 1980). Interestingly these structural units along the grain boundaries are also found to be a preferred segregation site for B (Hashimoto *et al.* 1984). These calculations indicate that a likely interstitial arrangement of B in these Fe defect structures is in one of the two sixfold trigonal prism sites of the structural unit (Hashimoto *et al.* 1984). This uncertainty in the exact position is reflected in the diagram (figure 2(b)) by placing the B in the centre of the diamond (between the two likely sites). From the modified  $4 \times 4 \times 1$  block of B2 cells, 14 units appear to be distorted FeAl units and two are Fe defect units (missing Al) that we propose contain interstitial B. Thus, the image indicates the composition of this precipitating phase is Fe<sub>16</sub>Al<sub>14</sub>B<sub>2</sub>.

Figure 3 is a Z-contrast image of the <100> projection of the precipitate. This is the view looking perpendicular to the long dimension of the rods and along one of the diagonals of the precipitate's square cross-section. The projected structure has the same periodicity and lattice spacing as that of the FeAl matrix. Also, if one considers any single bright feature (corresponding to an atomic column) and its four nearest neighbours, the precipitate phase appears to be similar to its B2 host. However, a more global view shows that there are bright stripes in this view of the precipitate, running parallel to the long axis [001] of the rods, that are not seen in the FeAl matrix. These bright stripes contain every fourth layer of the B2-like cells (two Fe planes separated by an Al plane) in the precipitate. This would indicate, as expected, that the lattice parameter of the precipitate in this direction <100> is four times that of FeAl, but this is somewhat surprising. In this projected view of the  $\nu$  phase, the diamond-like features seen looking down the long axis of the rods are contained in every other layer of B2 cells. They would be alternating between two different orientations but, if the diamond units are symmetric, they should look identical in this projection. This would mean that every other B2 layer has different scattering intensities. That we see every fourth layer bright may be an indication that the diamond units are asymmetrically distorted by the presence of B. It is also possible that the lines of extra intensity are the result of detector asymmetries or tilt of the sample. Additional work is required to resolve this issue.

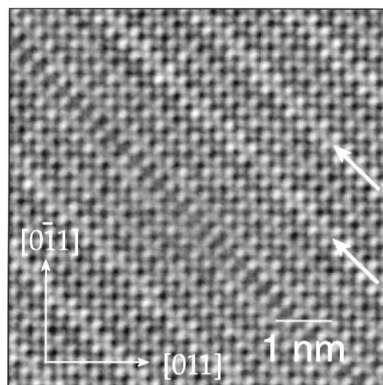


Figure 3. Z-contrast image of the <100> projection of the precipitate. This is the view looking perpendicular to the long dimension of the rod-like precipitates and along one of the diagonals of the precipitate's square cross-section. Every fourth layer (white arrows) of B2-like cells appears brighter. The stacking fault at the centre of the precipitate can be seen to involve a region three B2 cells wide.

The fault at the centre of the precipitate can be seen to involve a region three B2 cells wide. A fault was always seen in the approximate centre of the precipitate. The fault runs along the diagonal of the square cross-section of the precipitates when looking down the long axis of the rod-like precipitates and down the length of the rods. There is evidence that the precipitates nucleate at the faults and that the fault persists as the precipitate grows (Pang and Kumar 1998).

EELS data confirm the presence of B (figure 4) in the rod-like precipitates. The B concentration can be quantified by comparing the intensity under the B-K edge with the intensity under the Fe- $L_{2,3}$  edge, weighted by the inelastic cross-section (Egerton 1996). The resulting B-to-Fe ratio in the  $\nu$ -phase precipitate is found to be  $0.15 \pm 0.03$ . This compares favourably with the B-to-Fe ratio of 0.125 suggested by the image.

Additionally, EELS data can be used to provide bonding information. The integrated intensity of the plasmon peaks is proportional to the ratio of the sample thickness to the transmitted electron mean free path (Mallis *et al.* 1988). We observe that the plasmon peak intensity from the precipitates is much smaller than that from the FeAl matrix (figure 5). The boride precipitates are not significantly thinner than the matrix that surrounds them; thus they must have a longer electron mean free path than that of the matrix. This would indicate that some of the electrons are more closely bound in the B-containing precipitate. A comparison of the fine structure of the  $L_{2,3}$  ionization edges of Fe in the precipitate with that in the FeAl matrix (figure

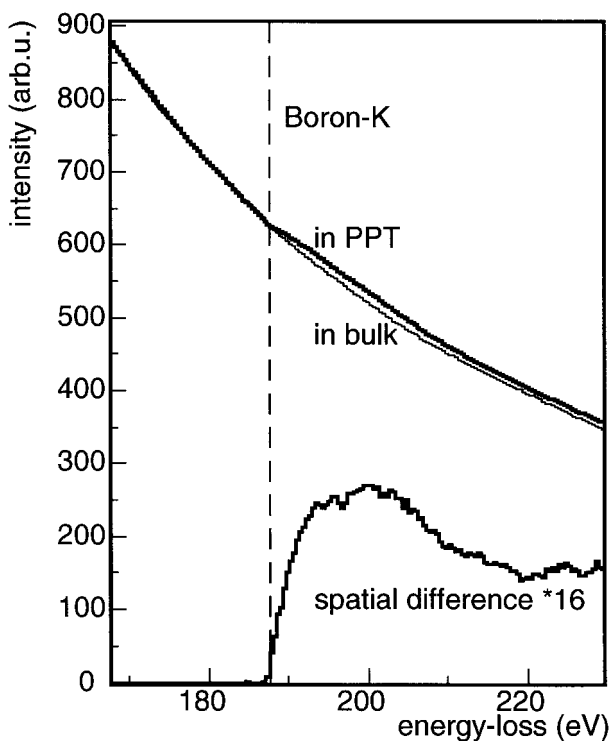


Figure 4. Electron-energy-loss spectra showing the presence of the B (B-K ionization edge) in the precipitates (PPT). The intensity of this edge is obtained by subtracting the spectrum obtained from the bulk.

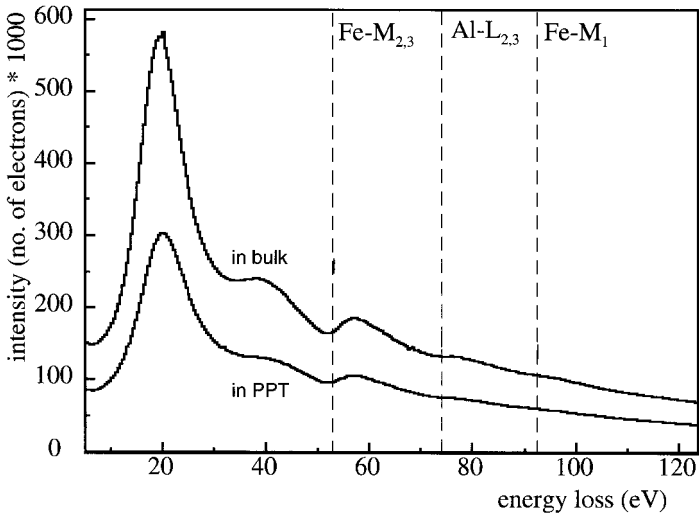


Figure 5. Valence loss region of electron-energy-loss spectra from a precipitate (PPT) and the matrix showing the plasmon peak (leftmost peak) and a number of ionization edges. The significant decrease in the plasmon peak intensity indicates that the valence electrons are bound more closely in the precipitates than in the matrix. Note that the two spectra shown here are on an absolute scale.

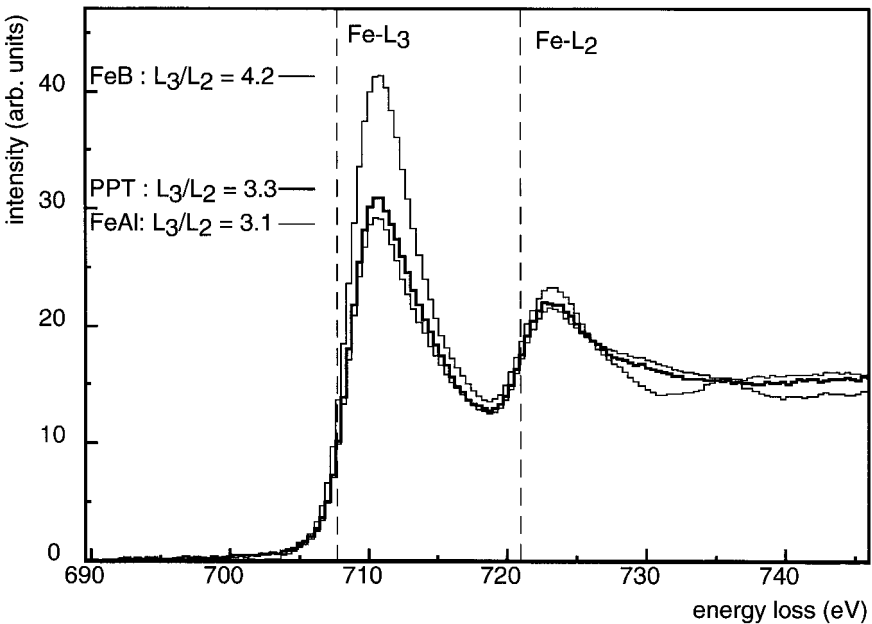


Figure 6. The Fe- $L_{2,3}$  ionization edges from an FeB grain-boundary particle, the B-containing precipitate and the FeAl matrix. All the spectra are normalized to the intensity of the Fe- $L_2$  peak. The precipitates show a small but significant increase of the  $L_3$ -to- $L_2$  ratio, indicating that the B is directly bonded to Fe.

6) reveals more empty d states in the precipitate (from the increase in the first peak of the  $L_3$  edge) (Pearson *et al.* 1988). The additional empty d states in the precipitate are attributed to the presence of the more electronegative B and suggests that Fe bonds directly to the B.

In addition to this second phase, there are also reports of platelet-like structures on (001) planes that have been variously ascribed to a second phase (Baker and Gaydos 1986), growth faults, (Song *et al.* 1991) or stacking faults arising from vacancy condensation (Yoshimi *et al.* 1996). High-resolution Z-contrast imaging showed that the platelets observed in this Fe-40 at.% Al-0.5 at.% B-0.7 at.% C alloy are Fe-rich faults (Fe-rich platelets). These structures have been discussed in detail by Pang *et al.* (1998).

The stability of these precipitates and faults has recently been investigated (Pang and Kumar 1998). Both are present in Fe-Al alloys containing B (Baker and Gaydos 1986, Crimp and Vedula 1986, Song *et al.* 1991, Yoshimi *et al.* 1996, Pierron and Baker 1997) or B and C (Pang and Kumar 1998); both form during cooling from 1150°C with intermediate cooling rates. The faults begin to disappear at about 600°C while the  $\nu$  phase is stable on heating to about 700°C.

#### §4. CONCLUSIONS

Z-contrast images provide a direct view of the atomic configuration in a recently discovered phase (designated  $\nu$  phase) found in Fe-Al alloys containing small B additions. The images reveal that the unit cell of this  $\nu$  phase is a modified  $4 \times 4 \times 1$  block of B2 unit cells. 14 of these B2 units appear to be distorted FeAl cells; the other two units are diamond-like (in the  $\langle 001 \rangle$  projection) arrangements of Fe that contain two six-coordinated trigonal prism sites, which are likely sites for interstitial B. Thus, from the images we deduce that the  $\nu$ -phase composition is  $\text{Fe}_{16}\text{Al}_{14}\text{B}_2$ . This B-to-Fe ratio of 0.125 suggested by the Z-contrast images compares favourably with the B-to-Fe ratio of  $0.15 \pm 0.03$  obtained from our EELS data. This new metastable boride phase has a much smaller metalloid content than seen in other known borides or carbides.

The structure of this boride corresponds to a superlattice of ordered vacancies on Al sites superimposed on the B2 matrix. We propose that the B2 order of the Fe and Al atoms is maintained with a superposition of ordered Fe defect structures (distorted B2 cells with a missing Al column) containing B interstitials. The strain produced by these distorted cells is more evenly dispersed by a uniform distribution of orthogonal defects.

#### ACKNOWLEDGEMENTS

This work was performed at Oak Ridge National Laboratory, which is managed by Lockheed Martin Energy Research Corporation for the US Department of Energy, under contract DE-AC05-96OR22464 and at Brown University. One author (G.D.) acknowledges the support provided by an appointment to the Oak Ridge National Laboratory Postdoctoral Program administered by the Oak Ridge Institute for Science and Education and Oak Ridge National Laboratory. Two of the authors (K.S.K. and L.P.) acknowledge the support provided by the Office of Naval Research under contract N00014-95-1-0564 with Dr S. G. Fishman as the program monitor.

## REFERENCES

- BAKER, I., and GAYDOSH, D. J., 1986, *Phys. Stat. sol. (a)*, **96**, 185.
- BAKER, I., LI, X., XIAO, H., CARLETON, R., and GEORGE, E. P., 1998, *Intermetallics*, **6**, 177.
- CRIMP, M. A., and VEDULA, K., 1986, *Mater. Sci. Engng*, **78**, 193.
- EGERTON, R. F., 1996, *Electron Energy-Loss Spectroscopy in the Electron Microscope* (New York: Plenum).
- GAYDOSH, D. J., DRAPER, S. L., and NATHAL, M. V., 1989, *Metall. Trans. A*, **20**, 1701.
- HASHIMOTO, M., ISHIDA, Y., YAMAMOTO, R., and DOYAMA, M., 1984, *Acta metall.*, **32**, 1.
- JESSON, D. E., and PENNYCOOK, S. J., 1993, *Proc. R. Soc. A*, **441**, 261.
- LIU, C. T., and GEORGE, E. P., 1990, *Scripta metall.*, **24**, 1285.
- MALLIS, T., CHENG, S. C., and EGERTON, R. F., 1988, *J. Electron Microsc. Techniques*, **8**, 193.
- NELLIST, P. D., and PENNYCOOK, S. J., 1999, *Ultramicroscopy*, **78**, 111.
- PANG, L., CHISHOLM, M. F., and KUMAR, K. S., 1998, *Phil. Mag. Lett.*, **78**, 349.
- PANG, L., and KUMAR, K. S., 1997a, *Phil. Mag. Lett.*, **76**, 323; 1997b, *Proceedings of the Second International Symposium on Structural Intermetallics*, 1997, edited by M. V. Nathal *et al.* (Warrendale, Pennsylvania: The Materials Society), p. 703; 1998, *Mater. Sci. Engng*, **258**, 161.
- PEARSON, D. H., FULTZ, B., and AHN, C. C., 1988, *Appl. Phys. Lett.*, **53**, 1407.
- PIERON, X., and BAKER, I., 1997, *High Temperature Structural Intermetallic Alloys VII*, Materials Research Society Symposium Proceedings, Vol. 460, edited by C. C. Koch *et al.* (Pittsburgh, Pennsylvania: Materials Research Society), p. 331.
- SONG, Z. Y., HASHIMOTO, H., CHOU, C. T., and ENDOH, H., 1991, *Phil. Mag. A*, **64**, 333.
- VITEK, V., SMITH, D. A., and POND, R. C., 1980, *Phil. Mag. A*, **41**, 649.
- YOSHIMI, K., HANADA, S., ONUMA, T., and YOO, M. H., 1996, *Phil. Mag. A*, **73**, 443.